Submitted to Physical Review Letters, April 2007

Lensless diffractive imaging using tabletop, coherent, high harmonic soft x-ray beams

Richard L. Sandberg, Ariel Paul, Daisy Raymondson, Steffen Hädrich, David Gaudiosi, Jim Holtsnider, Ron Tobey, Oren Cohen, Margaret. M. Murnane and Henry C. Kapteyn

JILA and Department of Physics, University of Colorado and NSF Engineering Research Center in Extreme Ultraviolet Science and Technology, Boulder, CO 80309, USA

Ph. (303) 210 – 0396; FAX (303) 492-5235; E-mail: Richard.Sandberg@colorado.edu

Changyong Song, Jianwei Miao

Department of Physics and Astronomy and California NanoSystems Institute, University of California, Los Angeles, California 90095, USA

Yanwei Liu, Farhad Salmassi

Center for X-ray Optics, Lawrence Berkeley National Laboratory, Berkeley, CA 94720, USA

Abstract

We present the first experimental demonstration of lensless imaging using a tabletop, coherent soft-x-rays source. A 29 nm high harmonic beam illuminates an object, and the diffraction is collected on an x-ray CCD camera. High dynamic range diffraction patterns are obtained by taking multiple exposures while blocking small-angle diffraction using beam blocks of varying size. These patterns reconstruct to images with 200 nm resolution. This work demonstrates a

practical tabletop lensless microscope that promises to find applications in materials science, nanoscience and biology.

Microscopy has proven to be a critical enabling technology for understanding biology and other physical sciences. Using innovative techniques, light microscopes can image living cells with a resolution as high as 200 nm [1]. However, this resolution is fundamentally limited by the wavelength of the visible/near-UV light. To further increase resolution, electrons can be used and atomic level resolution has been demonstrated in electron microscopy [2]. However, electron microscopes are limited by the mean-free-path of the charged particles, and as a result this technique is restricted to imaging thin samples, typically < 500 nm. Many biological specimens, as well as samples of interest for materials science, are too thick for electron microscopy. Furthermore, low contrast in electron microscopy also requires sophisticated labeling techniques. Thus, new techniques for nano-microscopy are of great interest.

One of the most promising alternative approaches for high-resolution imaging of thicker samples is to use shorter wavelength light, in the extreme ultraviolet (EUV) or soft-x-ray (SXR) regions of the spectrum [3]. EUV/SXR light can be used for nondestructive imaging applications requiring high resolution in thick samples [4]. Furthermore, numerous core-shell absorption edges and widely varying elemental absorption cross sections provide excellent inherent image contrast, in particularly for biological imaging in the "water window" (300 eV – 500 eV) region of the spectrum, or for magnetic domain imaging around 800 eV [3,5-6]. Successful soft-x-ray imaging techniques use diffractive or reflective optics such as Fresnel zone plates or multilayer mirrors since the very strong absorption by matter and low index contrast of materials at short wavelengths precludes the use of refractive optics. Zone-plate imaging has been demonstrated at

resolutions as high as 15 nm using state-of-the-art diffractive optics at synchrotron sources [7], while zone plate imaging with tabletop high harmonic sources can achieve resolutions of ≈ 200 nm [8]. Zone plates require very careful manufacturing, with feature sizes equal to the desired resolution, and dimensional tolerances several times smaller than this. Furthermore, microscopes based on zone plate optics have a relatively short depth of field.

Lensless imaging is a relatively new coherent imaging technique that is complementary to zone-plate imaging [9-13]. It is an extension of holography, which was first demonstrated with x-rays in 1987 [14]. This technique requires spatially coherent beams and eliminates imaging elements in the optical system by replacing them with a computerized phase retrieval algorithm. By obviating the need for an imaging system, lensless imaging is well-suited to x-rays, and was first demonstrated in 1999 using spatially-filtered light from a synchrotron source [9]. Also, lensless imaging has recently been demonstrated at a soft-x-ray free-electron laser [15]. In lensless imaging, the x-ray beam illuminates an object, and the diffracted light from the object is collected on an x-ray CCD camera. For the technique to work the diffraction pattern must be over sampled, i.e. the diffraction peaks coming from the highest resolution of interest must be sampled at higher than the Nyquist criterion [15]. If a sharp diffraction pattern has been obtained and the oversampling requirement is met, the image can be reconstructed using iterative algorithms [16].

High harmonic generation in gas-filled waveguides generates spatially coherent EUV beams and is ideally suited for lensless imaging [18,19]. This light source has already been used for Gabor holography with resolution < 10 μm [18]. Although Gabor holography and lensless imaging are

both coherent imaging techniques, geometric and flux considerations make lensless imaging better suited to high resolution imaging in a compact geometry. Here, we present the first experimental demonstration of lensless imaging using a tabletop source of coherent soft-x-rays. By taking multiple exposures while blocking small-angle scatter light using beam blocks of varying size, we obtain very high dynamic range diffraction patterns which successfully reconstruct to images with resolution near 200 nm. Moreover, no low spatial frequency information is missing from the reconstructions. This work thus demonstrates that lensless diffractive imaging can be successfully implemented using tabletop light sources, with broad potential application in nanoimaging and biological imaging.

The set-up is shown in Fig. 1. In our experiment, 1.3 mJ, 25 fs, femtosecond pulses from a Ti:sapphire laser amplifier systems (KMLabs DragonTM) are focused into a gas-filled waveguide at intensities of $5x10^{14}$ Wcm^{-2}. Phase matching of the conversion process is achieved by pressure tuning the gas. In this regime, bright emission over a comb of odd-order harmonics from 25 – 31 is obtained [20,21]. The hollow waveguide is a 150 μm inner-diameter, 10 cm long fused silica capillary filled with argon gas at ~65 Torr pressure. When optimally coupled, an EUV beam is generated with a beam waist of about 25 μm and approximately 1 milliradian divergence, and a flux of ~10^{12} photons per second in ~5 harmonics near 30 nm wavelength. Two 200 nm thick aluminum filters are used to eliminate the fundamental laser light, with the second being held in a specially designed light-tight fixture. A pair of narrowband, Mo/Si multilayer mirrors centered at ~29 nm acts as both a monochromator and a condenser, to gently focus the beam onto the sample with a beam diameter of a few hundred microns. The narrowband mirrors each have a reflectivity of 25% in a 2.5 nm bandpass, making it possible to effectively select a

single harmonic order. The sample is held in an x-y stage controlled by high-precision closed-loop dc motors. The diffraction of the EUV light from the sample is recorded on a large-area x-ray CCD camera (Andor) with a 2048 x 2048 array of 13.5 μm pixels.

Beam blocks of varying size are placed in the center of the diffraction pattern to block the more intense diffraction coming from low spatial frequencies. A large-diameter beam block (>1 mm diameter) allows us to acquire long exposure images to record the highest spatial frequencies diffracted from the sample, while a small beam block (<200 μm diameter) is used to record low spatial frequencies. These diffraction patterns are then stitched together, extending the dynamic range of the pattern from 4 to 12 orders of magnitude. These beam blocks are supported by a 12.5 μm wire tethered to a 2" diameter mounting ring. The mounting ring sits in a kinematic piezo controlled x-y lens translator to allow fine control of the beam block position.

A high quality and uniform soft-x-ray mode is needed for lensless imaging, to ensure the highest spatial coherence and sharpest diffraction data. Figure 1 shows the mode of the 29 nm beam after reflecting from the two multilayer mirrors. The mode profile fits to a near-perfect Gaussian, to the full dynamic range of the camera ($\approx 10^4$). The sample is carefully placed to optimize the illumination, diffraction quality, and oversampling ratio. To obtain a flatter intensity field and ensure long-term illumination stability, the illumination spot was kept large compared with the object. The sample must be placed far enough from the detector to guarantee a far field diffraction pattern, given by $z > \frac{D^2}{\lambda}$, where z is the sample to CCD distance, D is the sample diameter, λ is the wavelength. Finally, the distance from the sample to the CCD is chosen to give an appropriate linear oversampling ratio (> 5) that allows for easily reconstructable diffraction

patterns [22]. The linear oversampling ratio relates the smallest diffraction pattern speckles to CCD pixels, and is given by $O = \frac{z\lambda}{dD}$, where z is the sample to CCD distance, λ is the wavelength, D is the sample diameter, and p is the pixel size of the CCD camera. For the two images described here, O~10. In the reconstructed image, each *image* pixel (not to be confused with a CCD pixel), corresponds to a size *d* given by $d = \frac{OD}{N}$, where D is the sample size, and N is the number of pixels. This image pixel size is thus the ultimate resolution for any given geometry. Another limit on the resolution, r, of the reconstruction is the spectral bandwidth, $\lambda/\Delta\lambda$ of the source, where $r \geq \frac{OD}{\lambda/\Delta\lambda}$ [20]. By looking at the fidelity of the diffraction pattern speckles near the edge of the CCD camera (high scattering angle) we estimate a lower bound on our spectral bandwidth of ≈ 200.

We used two objects for these initial experiments: a rectangular "J" aperture with a length of 80 μm, and a 15 μm diameter apertured section of a thin carbon foil with holes of various sizes ("Quantifoil Multi-A"). For the "J" object, the O was 9, with a sample to CCD distance z = 33 cm, and a sample size D = 80 μm. This results in an image resolution of < 1 μm. For the thin carbon film (~ 40 nm), O = 13, z = 9 cm and the sample size d was 15 μm. Figure 2(a) shows the coherent diffraction pattern from the "J" slit, which is slightly non-centro-symmetric due to the absorption by the sample. Three different diffraction patterns were stitched together to form the high dynamic range data. The lowest spatial frequencies were captured with no beam block in about 1 minute. Next, a small beam block, ~ 200 μm in diameter, was used with ~10 min exposure. Finally, a larger beam block, ~3 mm in diameter, was used to capture the highest spatial frequencies in ~120 minutes.

To reduce noise in the final diffraction patterns, we applied the inverse Fourier transform to obtain the autocorrelation function of the sample. Since the linear oversampling ratio is much higher than 2, the autocorrelation function is surrounded by a large region that should have no signal. However, because of camera noise that region is not exactly zero. We therefore applied a low-pass filter to force this region to be zero. We then numerically integrated the diffraction pattern intensity by binning 3×3 pixels into 1 pixel and applying a deconvolution to remove the artifacts in the diffraction pattern due to intensity integration [23]. Only the central 2040 x 2040 pixels were used for this integration. This step significantly enhanced the signal-to-noise ratio of the coherent diffraction pattern. The analyzed diffraction pattern has a linear oversampling ratio ~1/3 smaller than stated above and an array size of 680 x 680 pixels. This also eases the requirement on the temporal coherence by a factor of 3.

Phase retrieval of the coherent diffraction pattern is carried out using the guided hybrid-input-output (GHIO) algorithm [23]. This algorithm starts with 16 independent reconstructions with random initial phases. Each reconstruction iterates back and forth between real and reciprocal space. In real space, the sample density outside a support and the negative real or imaginary part of the electron density inside the support are slowly pushed to zero. The support is a rectangular shape with its size estimated from the linear oversampling ratio. In reciprocal space, the magnitude of the Fourier transform (*i.e.* square root of the diffraction intensity) remains unchanged, and the phase is updated with each iteration. After 2000 iterations, 16 images are reconstructed, and an R-value is calculated for each based on the difference between the measured and calculated Fourier transform magnitude. The image with the smallest R-value is

used to obtain a new set of 16 images for the next generation. After the 8^{th} generation, the 16 reconstructed images became consistent. Based on the reconstructed images, we define a tight support that represents the true envelope of the object. Using this tight support, we start with another GHIO run and obtain the final reconstructed image. Because the diffraction pattern is non-centro-symmetric, the electron density of the sample is complex, which in principle makes the phase retrieval more difficult than for real objects. By using a tight support with GHIO, and imposing a positivity constraint on both the real and imaginary parts, we have shown that complex objects can be reliably reconstructed.

Figure 2(b) shows the final image of the J pattern, with each pixel corresponding to 347 nm. The reconstructed image is consistent with the optical microscope image shown in Fig. 2(a). A lensless image of the carbon film, apertured to 15 μm, is shown in Fig. 3. Figure 3(a) is a SEM picture of the sample, and 3(b) shows its diffraction pattern. The non-centro-symmetry of the diffraction pattern indicates that the sample has absorption and that the sample density is complex. Figure 3(c) shows the real part of the sample density for the final image, which agrees well with the SEM image. A line scan of the reconstructed image indicates that the current tabletop lensless microscope has a resolution of 214 nm.

Three approaches are possible for further improving the ultimate resolution of the microscope. First, a larger detector would allow higher spatial frequencies to be captured while maintaining O. Second, the effective source spectral bandwidth could be improved using narrower band mirrors and/or by narrowing the individual harmonic peaks. Third, shorter wavelength HHG light could be used. Techniques for quasi phase matching, and selective enhancement of a single

harmonic order, have recently been demonstrated that allow for the efficient generation of shorter wavelength harmonics, while also accomplishing spectral selectivity that reduces the need for filtering, and thus will increase the throughput of the condenser optics [24-26]. These improvements are quite feasible, and will increase the ultimate resolution to 10's of nm. As the laser repetition rates are increased from 3 kHz to tens of kHz, the soft-x-ray flux will be simultaneously increased, and image acquisition time will be dramatically reduced. As computing power increases and reconstruction times shrink, such a lensless microscope will become increasingly practical for routine use in biological imaging, nanoscience, and metrology in support of next-generation lithographies. Moreover, the short duration of high harmonics allows time-resolved imaging on femtosecond timescales.

Several aspects of lensless imaging make it extremely elegant and appealing. Our light source, while bright, does not compete with the flux available at a synchrotron or FEL. Thus, ease of sample setup is an important concern. Because lensless imaging only requires illumination with a plane wave, placement of the sample is non-critical. No multi-step focusing process is necessary, as is the case for zone-plate imaging. Furthermore, although zone plata microscopes rely on geometrical magnification and thus are often quite large, our entire imaging apparatus fits in 0.5 m x 1.5 m.

The authors would like to acknowledge the invaluable help of the JILA Instrument Shop as well as assistance from the Lehnert labs. R.L. Sandberg acknowledges support from an NSF IGERT fellowship. The authors gratefully acknowledge funding from the NSF ERC for Extreme

Ultraviolet Science and Technology under NSF Award No. 0310717 and Department of Energy NNSA. JM acknowledges funding from NSF and DOE.

References

[1] S. M. Hurtley and L. Helmuth, Science **300**, 75 (2003).

[2] J. C. H. Spence, *Experimental High-Resolution Electron Microscopy*, 3rd ed. (Oxford University Press, New York, 2003).

[3] D. Attwood, *Soft X-rays and Extreme Ultraviolet Radiation: Principles and Applications* (Cambridge University Press, Cambridge, 1999).

[4] C. A. Larabell and M. A. Le Gros, Mol Biol Cell **15**, 957 (2004).

[5] P. Fischer *et al.*, Materials Today **9**, 26 (2006).

[6] S. Eisebitt *et al*., Nature **432**, 885 (2006).

[7] W. Chao *et al.*, Nature **435**, 1210 (2005).

[8] M. Weiland *et al.*, Ultramicoscopy **102**, 93 (2005).

[9] J. Miao *et al.*, Nature **400**, 342 (1999).

[10] D. Shapiro *et al.*, Proc. Natl. Acad. Sci. USA **102**, 15343 (2005).

[11] M. A. Pfeifer *et al.*, Nature **442**, 63 (2006).

[12] H. M. Quiney *et al.*, Nature Phys. **2**, 101(2006).

[13] X. Xiao and Q. Shen, Phys. Rev. B **72**, 033103 (2005).

[14] J. E. Trebes *et al.*, Science **238**, 517 (1987).

[15] H. N. Chapman *et al.*, Nature Phys. **2**, 839 (2006).

[16] J. Miao *et al.*, J. Opt. Soc. Am. A **15,** 1662 (1998).

[17] J. R. Fienup, Appl. Opt. **21**, 2758 (1982).

[18] R. A. Bartels *et al.*, Science **297**, 376 (2002).

[19] X. Zhang *et al.*, Opt. Lett. **29**, 1357 (2004).

[20] A. Rundquist *et al.*, Science **280**, 1412 (1998).

[21] H. C. Kapteyn, M. M. Murnane, and I. P. Christov, Phys. Today, March Issue (2005).

[22] J. Miao *et al.*, Phys. Rev. B **67**, 174104 (2003).

[23] C. Song *et al.*, Phys. Rev. B **75**, 012102 (2007).

[24] A. Paul *et al.*, Nature **421**, 51 (2003).

[25] X. Zhang *et al.*, Nature Phys. **3**, 270 (2007).

[26] A. Lytle *et al.*, Phys. Rev. Let. **98**, 123904 (2007).

Figure Captions

FIG. 1. Experimental setup for lensless imaging using coherent high harmonic beams at a wavelength of 29 nm. A single harmonic order is selected and focused using a pair of normal-incidence multilayer mirrors. The sample stage is positioned near the focus, where it scatters the soft-x-ray beam onto a CCD. Beam blocks of varying size are used to obtain high dynamic range. Inset, measured logarithmically scaled soft-x-ray beam profile that is a near-Gaussian TEM_{00} over 4 orders of magnitude.

FIG. 2. Object, diffracted pattern, and reconstructed image. (a) Optical image of 'J'-slit. (b) Oversampled diffraction pattern from this sample. (c) Magnitude of the reconstructed lensless image. Detailed structural imperfections near the edges of the slit are recovered in the reconstructed image.

FIG. 3. (a) SEM image of a masked carbon film; (b) oversampled soft-x-ray diffraction pattern; and (c) magnitude of the reconstructed lensless image. The correspondence in size, number and position of holes, and aspect ratios between the EUV image and the SEM image is excellent. One pixel in the reconstructed image corresponds to 107 nm. The inset in (c) show a line-scan taken along the direction noted with the green solid line, demonstrating a spatial resolution of 214 nm. The reconstructed image in (c) is flipped and tilted for a direct comparison with the SEM image in (a).

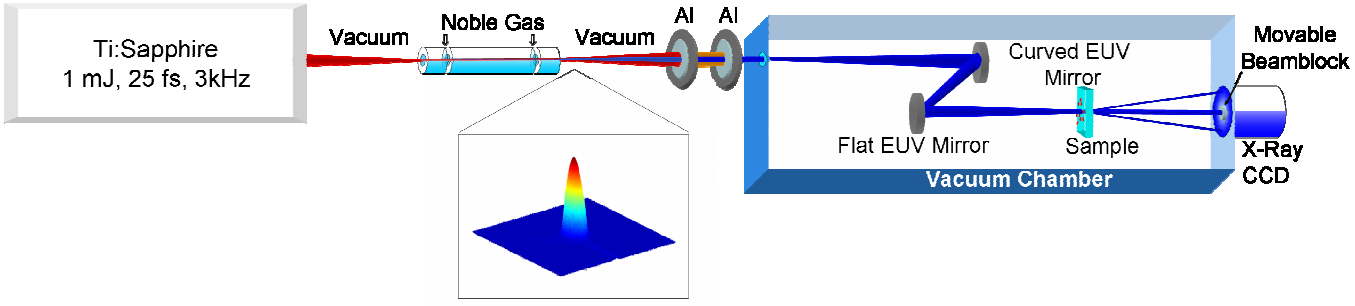
Ti:Sapphire
1 mJ, 25 fs, 3kHz
Vacuum
Noble Gas
Vacuum
Al
Al
Curved EUV
Mirror
Movable
Beamblock
Flat EUV Mirror
Sample
X-Ray
CCD
Vacuum Chamber

FIGURE 1

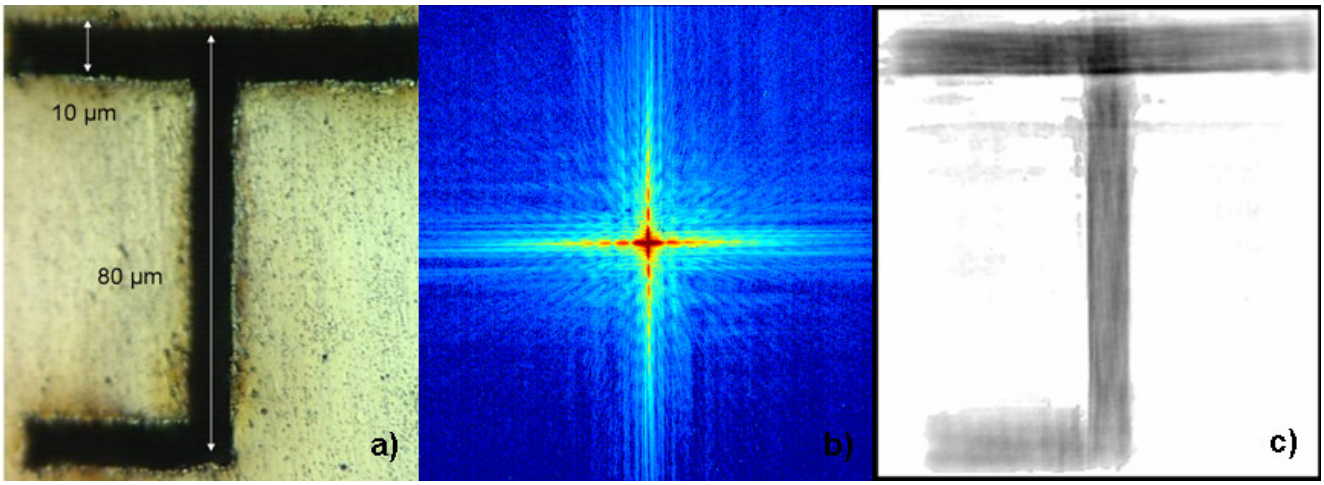

FIGURE 2

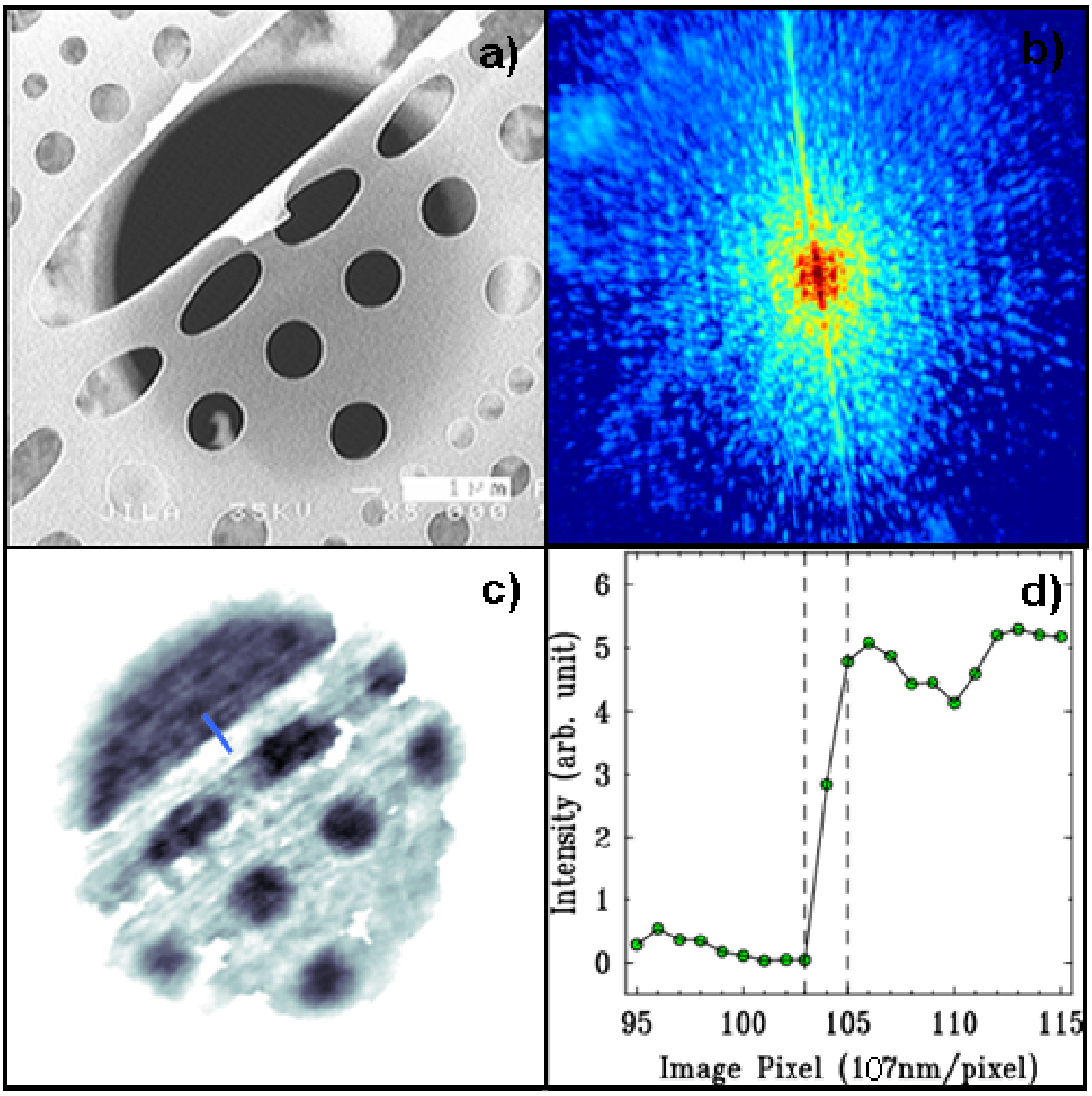
a)
b)
c)
d)
Intensity (arb. unit)
0
1
2
3
4
5
6
95
100
105
110
115
Image Pixel (107nm/pixel)

FIGURE 3